

RESEARCH ARTICLE | MARCH 07 2007

Time-resolved spectroscopy of silver nanocubes: Observation and assignment of coherently excited vibrational modes

Hristina Petrova; Chien-Hua Lin; Suzanna de Liejer; Min Hu; Joseph M. McLellan; Andrew R. Siekkinen; Benjamin J. Wiley; Manuel Marquez; Younan Xia; John E. Sader; Gregory V. Hartland



J. Chem. Phys. 126, 094709 (2007)

<https://doi.org/10.1063/1.2672907>



View
Online



Export
Citation

CrossMark

Articles You May Be Interested In

Multi-frequency ferromagnetic resonance investigation of nickel nanocubes encapsulated in diamagnetic magnesium oxide matrix

J. Appl. Phys. (December 2016)

Phase transformation of FeO / Fe₃O₄ core/shell nanocubes and facile synthesis of Fe₃O₄ nanocubes

J. Appl. Phys. (April 2010)

Synthesis of core-shell nanocubes for higher SERS enhancement

AIP Conference Proceedings (July 2019)

500 kHz or 8.5 GHz?
And all the ranges in between.

Lock-in Amplifiers for your periodic signal measurements



Find out more

 Zurich
Instruments

Time-resolved spectroscopy of silver nanocubes: Observation and assignment of coherently excited vibrational modes

Hristina Petrova

Department of Chemistry and Biochemistry, University of Notre Dame, Notre Dame, Indiana 46556-5670

Chien-Hua Lin and Suzanna de Liejer

Department of Mathematics and Statistics, The University of Melbourne, Victoria 3010, Australia

Min Hu, Joseph M. McLellan, Andrew R. Siekkinen, and Benjamin J. Wiley

Department of Chemistry, University of Washington, Seattle, Washington 98195-1700

Manuel Marquez

NCTCN Center, Physical and Chemical Properties Division, NIST, Gaithersburg, Maryland 20899

Younan Xia

Department of Chemistry, University of Washington, Seattle, Washington 98195-1700

John E. Sader

Department of Mathematics and Statistics, The University of Melbourne, Victoria 3010, Australia

Gregory V. Hartland

Department of Chemistry and Biochemistry, University of Notre Dame, Notre Dame, Indiana 46556-5670

(Received 15 November 2006; accepted 17 January 2007; published online 7 March 2007)

The response of single crystal, cubic silver particles to ultrafast laser-induced heating has been examined experimentally and theoretically. The transient absorption traces display clear modulations due to coherently excited vibrational modes. Nanocube samples with edge lengths smaller than 50 nm show a single modulation, whereas samples larger than 50 nm show two vibrational modes. The results are compared to finite element calculations, where the cubes are modeled as having cubic crystal symmetry with the principal axes parallel to the sides of the particle. The action of the laser pulse is treated in two ways, first, as creating a uniform initial strain. In this case the predominant mode excited is the breathing mode. The period of this mode is in reasonable agreement with the vibrational periods measured for the smaller cubes and with the higher frequency modulation observed for the larger cubes. A nonuniform initial strain is also considered, which could arise from nonuniform heating for particles larger than the optical skin depth of the metal. In this case the predominant mode excited is a nontotally symmetric mode. The calculated periods from this analysis are in reasonable agreement with the lower frequency modulations observed for the larger samples. The results from this study show that, to within the accuracy of these measurements, the elastic constants of cubic silver nanoparticles are the same as bulk silver. © 2007 American Institute of Physics. [DOI: [10.1063/1.2672907](https://doi.org/10.1063/1.2672907)]

I. INTRODUCTION

Understanding how the properties of materials change with size has been a long-standing problem in physical science—dating back to the turn of the last century.¹ The properties that have been studied include phase transition temperatures^{2–4} and pressures,^{5,6} changes in the band gap for semiconductors,^{7,8} and the catalytic activity of small metal particles.^{9–11} These studies have been traditionally limited to particles that have roughly spherical symmetry. Recently, a number of synthetic techniques have been developed to produce high quality (narrow size distribution) samples of rods,^{12–14} triangles,^{15,16} and cubes and boxes,¹⁷ as well as more exotic shapes such as tetrapods,^{18,19} branched particles,²⁰ and stars.²¹ These particles grow with very specific crystalline structures, which allows exploration of how shape and crystal structure, as well as size, affects the properties of materials.

Over the past several years we, and several other groups, have used time-resolved spectroscopy to examine the elastic properties of nanoparticles.^{22–26} In these experiments ultrafast laser-induced heating coherently excites the vibrational modes of the particle that map onto the expansion coordinate. These modes produce a modulation in the transient absorption traces.^{22,23} Comparing the measured periods to continuum mechanics calculations yields information about the elastic constants of the particles, if the size and shape are known.^{22–26} Most studies have been concerned with metallic systems,^{22,23,25,26} although similar experiments can be performed on semiconductors.^{24,27} For spherical metal particles these experiments show that the elastic constants are the same as the bulk material.^{22,23} These particles are polycrystalline and, therefore, elastically isotropic.²⁸ Coherently excited vibrational modes have also been observed for triangular silver particles,²⁶ which grow as single crystals.¹⁵ A good match was found between the experimentally mea-

sured periods and the periods calculated using the bulk elastic constant data. In contrast, experiments with gold nanorods show that the value of Young's modulus for these materials is approximately 20%–30% lower than that for bulk gold.^{23,29,30} The nanorods grow in very specific ways—as either single crystals with a [100] growth direction^{31–33} or as pentatwinned crystals with a [110] growth direction.^{34–36} The transient absorption results are difficult to explain in terms of the structure of the nanorods, which has motivated us to study other single crystal nanoparticle systems of different shapes.

In this paper we present experimental transient absorption data and theory for silver nanocubes. These particles are single crystals with {100} facets.¹⁷ They have edge lengths between 30 and 100 nm, with typical standard deviations for the size distribution of 10%–15%. Coherently excited vibrational modes can be clearly seen in the transient absorption traces. The results from the experiments are compared to numerical calculations, which are described in detail below. The calculations predict that the dominant mode excited in these experiments should be the breathing mode of the cube. However, the experimental data for the larger samples show two modulations. The high frequency motion is consistent with the breathing mode. The low frequency motion is assigned to a nontotally symmetric mode that is excited by nonuniform heating of the particles. Such an effect may arise from the finite optical penetration depth of the pump laser.³⁷

II. EXPERIMENTAL PROCEDURES

The silver nanocubes were prepared using a slightly modified version of the polyol synthesis described in Ref. 38. Briefly, 5 ml of ethylene glycol (EG) (J. T. Baker) was added to a disposable 6 dram glass scintillation vial (VWR international) and heated in an oil bath at 145 °C for 1 h. 0.5 ml of a 3 mM solution of HCl (J. T. Baker) in EG was then added. After 10 min, solutions of AgNO₃ (1.5 ml of a 94 mM solution in EG, Aldrich) and poly(vinyl pyrrolidone) (PVP) (1.5 ml of a 147 mM solution in EG, molecular weight ≈55 000, Aldrich) were injected at a rate of 22.5 ml/h using a dual channel syringe pump (KDS-200, Stoelting, Wood Dale, IL). Following injection of the AgNO₃ and PVP the vial was loosely capped. The solution was left in this state for over a day, at which point the vial was sealed. After sealing, the solution gradually turned dark yellow, then reddish-brown, and finally thick greenish-gray. The final size is determined by the total reaction time.³⁸ Magnetic stirring at 350 rpm was applied throughout the synthesis. The product was washed and collected by centrifugation for 30 min at 3900 rpm, first with acetone to remove EG then at least twice with water to remove excess PVP. Cubes were the primary product in this synthesis (>95%), and they formed stable suspensions in water without any additional stabilizers.

The samples were analyzed by scanning electron microscopy (SEM) and transmission electron microscopy (TEM). Specimens for SEM were prepared by placing small drops of the dispersions of metal nanoparticles on silicon substrates (Silicon Valley Microelectronics, San Jose, CA). Copper

grids coated with amorphous carbon (Ted Pella, Redding, CA) were used for TEM. The samples were allowed to dry at room temperature in a fume hood. The SEM images were obtained using a field-emission microscope (Sirion XL, FEI, Hillsboro, OR) operated at 15 kV. The TEM images were taken using a Philips 420 electron transmission microscope operated at 120 kV. UV-vis absorption spectra were taken with a Cary 50 UV-vis spectrometer.

The transient absorption experiments were performed with a regeneratively amplified Ti:sapphire (Clark-MXR, CPA-1000). Pump pulses at 400 nm were produced by second harmonic generation and probe pulses in the visible region were obtained from a white-light continuum. Transient absorption traces at specific probe wavelengths were collected as a function of pump-probe delay. Fluctuations in the intensity of the probe were normalized on a shot-to-shot basis using boxcars integrators, in combination with an analogue division integrated circuit and a lock-in amplifier. Time and wavelength resolved data were also collected using an Ultrafast Systems UV-visible femtosecond spectrometer, with a Clark-MXR CPA-2010 laser as the pump source.

The samples were contained in 1 mm path length cuvettes for the transient absorption experiments, and the experiments were performed without flowing. The laser spot size at the sample in these experiments was between 2 and 4 mm². The transient absorption signal showed a slight decrease in magnitude, but no change in form during the course of the experiments, indicating that laser-induced damage of the samples is not significant. The period of the coherently excited vibrational modes was obtained by fitting the modulated portion of the data to a damped cosine function with a decaying offset, using the “SOLVER” routine in MICROSOFT EXCEL. Note that the ability to collect time and wavelength resolved data with the Ultrafast Systems spectrometer is a tremendous advantage for assigning signals in these experiments. However, the ultimate signal to noise in this system is not as good as that of the single wavelength detection scheme. This is primarily because the single wavelength scheme employs shot-to-shot normalization. Thus, the majority of the data in this paper were collected with the single wavelength detection scheme.

III. RESULTS AND ANALYSIS

A. Experimental results

Figure 1 shows representative SEM and TEM images of the nanocubes used in the transient absorption experiments (note the different scale bars for the different images). The average dimensions of the particles determined from analysis of the TEM images are collected in Table I. Approximately 200–400 particles were counted for each sample (the exact number is given in Table I). The errors given for the size in Table I represent the standard deviation. The samples are fairly uniform in size, with standard deviations on the order of 10%–20%. Figure 2 shows UV-vis absorption spectra of selected cube samples (samples S1, S4, S5, and S6). The spectra show a broad band in the visible region due to the surface plasmon resonance (SPR) of the cubes. The SPR shifts to the red and broadens as the size of the particles

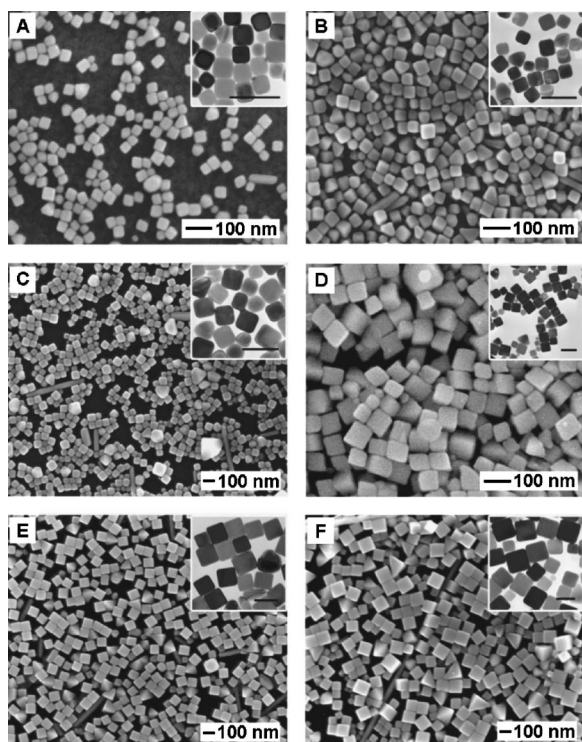


FIG. 1. SEM and TEM images (inserts) of the different nanocube samples used in these experiments. Panels A–F correspond to samples S1–S6. Note the different sizes of the scale bars in the images. The average edge lengths for each sample are collected in Table I.

increases—consistent with increasing contributions from re-radiation effects and radiation damping with increasing size.³⁹

Figure 3 shows time and wavelength resolved transient absorption data for sample S4. The top panel shows the full contour plot of the data and the bottom panel shows a transient absorption trace at 448 nm [extracted from the data in Fig. 3(a)]. Modulations that correspond to coherently excited vibrational modes can be clearly seen in both the contour plot and the single wavelength trace.^{22,23,26,40} The contour plot shows a complicated behavior. At wavelengths to the red of 500 nm a single modulation is observed. The period decreases slightly as the probe wavelength decreases. This decrease is attributed to the polydispersity in the sample.⁴¹

TABLE I. Average values of the edge length and period for the different nanocube samples. The samples are arranged in order of increasing edge length. The errors represent the standard deviation. The number of particles counted in the TEM measurements for samples S1–S6 were 421, 271, 284, 415, 188, and 465.

Sample	Length (nm)	Period (ps)
S1	35.5±3.4	19±1
S2	38.6±3.9	22±1
S3	48.1±7.5	28±1
S4	54.2±11.2	30±3 38±2
S5	72.1±11.2	44±1 57±2
S6	85.6±18.1	42±4 62±1

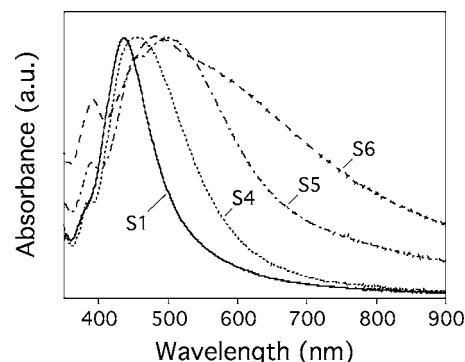


FIG. 2. UV-vis absorption spectra of selected nanocube samples S1, S4, S5, and S6. The average edge lengths for the samples are 35, 54, 72, and 86 nm, respectively.

Larger cubes absorb in the red part of the spectrum and smaller cubes absorb at blue wavelengths (see Fig. 2),⁴² thus, as the probe wavelength is tuned from the red to the blue we select smaller cubes and see a faster period. At probe wavelengths less than 500 nm two modulations are observed. This is illustrated in the 448 nm trace presented in Fig. 3(b). This trace cannot be fitted using a single cosine function. The two cosine terms extracted by the fitting procedure are shown above the experimental data. The two modulations have similar amplitudes, but a different phase at this wavelength (phase difference=120°). Also note that the damping time of the modulations is faster for the higher frequency component.

Figure 4 shows transient absorption traces for sample S6 (the largest sample). Two modulations can also be clearly seen in this trace. In comparison to sample S4, the amplitudes for the two modulations are again similar, but they are in phase at this probe wavelength (the phase difference is only 10° for this trace). The higher frequency modulation for sample S6 has a faster decay time compared to the lower frequency component, similar to that observed for sample S4. Sample S5 also shows two modulations (data not presented), however, the lower frequency component is much weaker in this case. The average periods determined from analysis of the experimental data are given in Table I, and are plotted against the average dimensions of the particles in Fig. 5. The errors reported in Table I and Fig. 5 are the standard deviations for the size and period measurements. The periods of both the modes are clearly proportional to the edge length.

B. Finite element analysis

In this section, we calculate the vibrational response of a silver cube following excitation by a thermal pulse. This is achieved in an analogous manner to that performed for rods in Ref. 43, by decomposing the initial strain into the natural vibration modes of the cube, which are calculated numerically. Finite element analysis is used⁴⁴ and the Fourier coefficients for both the deformation and change in volume are obtained. We consider a cube composed of a linearly elastic material that is anisotropic with cubic crystal symmetry. The principal crystal axes of the cube are parallel to the edges—which is appropriate for cubes with {100} faces.¹⁷

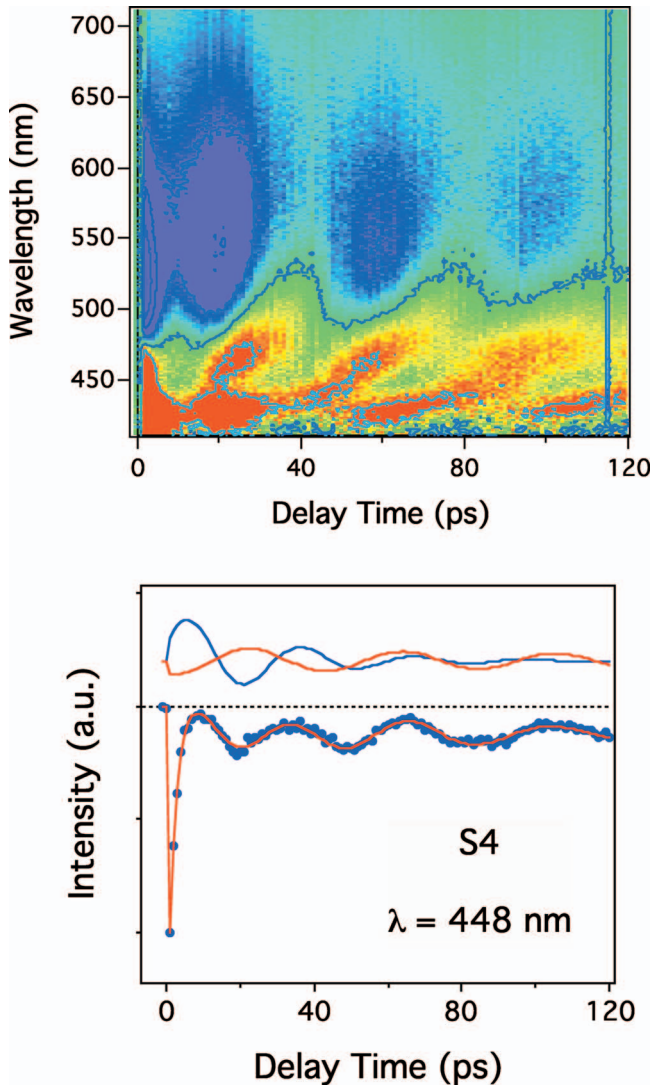


FIG. 3. (Color) (a) Top: contour plot of the wavelength vs time response for sample S4. Blue/purple=positive signal and red=negative signal. (b) Transient absorption trace at $\lambda=448$ nm extracted from the data in (a). The solid lines show a fit to the data using two cosine terms and exponential decays for electron-phonon coupling and heat dissipation. The two cosine components extracted from the fit are shown above the experimental trace.

As in Ref. 43, we consider the thermal pulse to be of infinitesimal duration, since the characteristic time for vibration greatly exceeds the time scale for energy flow from the hot-electron distribution created by the pump laser into the lattice (several picoseconds). In addition, since the time scale for heat transfer from the particle to the surroundings is much longer than the vibration period,⁴⁵ the cube is considered to remain at constant temperature following excitation. We initially assume that the thermal pulse acts to heat the cube uniformly, as such the initial state of the cube relative to its final state after application of the pulse is that of a uniform strain, i.e.,

$$U_{t=0} = -\varepsilon(x\hat{x} + y\hat{y} + z\hat{z}), \quad (1)$$

where U is the displacement vector, x , y , and z are the components of the Cartesian coordinate, \hat{x} , \hat{y} and \hat{z} are the unit vectors for each Cartesian axis, ε is the magnitude of the initial strain, and t is time. Importantly, the displacement

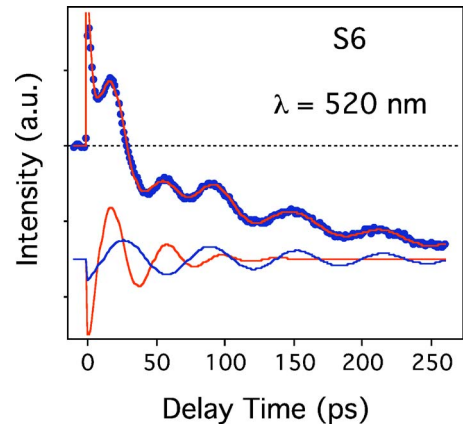


FIG. 4. Transient absorption data for sample S6 recorded at $\lambda=520$ nm. The solid line shows a fit to the data using two cosine terms and exponential decays to describe electron-phonon coupling and heat dissipation. The two cosine components extracted from the fit are shown below the experimental trace.

vector is taken with respect to the final equilibrium state, which coincides with the average shape of the cube following excitation. We will later relax the assumption of uniform initial strain to investigate the effect of nonuniform heating resulting from the finite penetration depth of the pump laser.

To evaluate the contributions for different modes, we note that the vibrational modes form a complete orthogonal basis set. We may therefore express the displacement of the cube as a linear combination over all modes:

$$U(x, y, z, t) = \sum_n \alpha_n \mathbf{u}_n(x, y, z) \exp(-i\omega_n t), \quad (2)$$

where the subscript n refers to the n -th mode, $\mathbf{u}_n(x, y, z)$ is the spatial displacement vector of each mode, ω_n is the radial resonant frequency of the n th mode, and α_n is the Fourier coefficient of the n th mode which is given by

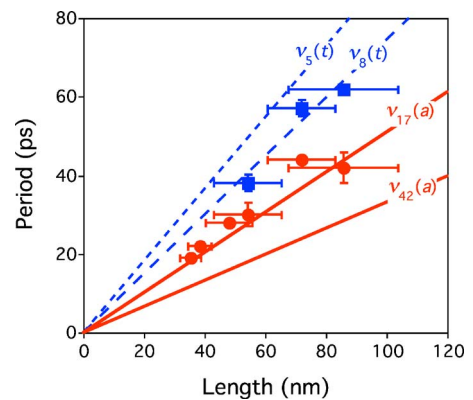


FIG. 5. Average period vs average edge length for all the samples examined. The solid lines are the calculated periods for the dominant modes excited by a uniform initial strain [$\nu_{17}(a)$ and $\nu_{42}(a)$]. The dashed lines are the calculated periods for the dominant modes excited by a nonuniform initial strain [$\nu_5(t)$ and $\nu_8(t)$]. The error bars indicate the standard deviation of the measurements.

$$\alpha_n = \int_V \mathbf{u}_n \cdot \mathbf{U}_{t=0} dV, \quad (3)$$

where the integral is performed over the volume of the cube and the modes are normalized such that $\int_V |\mathbf{u}_n|^2 dV = 1$.

Noting that displacements are infinitesimal within the framework of the theory of linear elasticity,²⁸ it then follows that the temporal response of the change in volume is given by

$$\frac{\Delta V}{V} = \sum_n \gamma_n \exp(-i\omega_n t), \quad (4)$$

where ΔV is the change in volume, V is the initial volume of the cube and

$$\gamma_n = \frac{\alpha_n}{a^3} \int_S \hat{\mathbf{n}} \cdot \mathbf{u}_n dS, \quad (5)$$

where $\hat{\mathbf{n}}$ is the outward normal unit vector to the surface of the cube, a is its side length, and the integration is performed over the surface of the cube. Since the change in the optical absorption spectrum in the measurements will be dictated by both deformation and volume changes, we present results from both these contributions. The integrals in Eqs. (2)–(5) were evaluated numerically by calculating the modes using finite element analysis. The finite element analysis requires the density, Young's modulus (E), Shear modulus (G), and Poisson's ratio (ν) for the different crystal directions in the cube. The specific formulas for $E_{[ij]}$, $G_{[ij]}$, and $\nu_{[ij]}$ are²⁸

$$E_{xx} = E_{yy} = E_{zz} = \frac{(C_{11} - C_{12})(C_{11} + 2C_{12})}{(C_{11} + C_{12})}, \quad (6a)$$

$$G_{xy} = G_{yz} = G_{xz} = C_{44}, \quad (6b)$$

$$\nu_{xy} = \nu_{yz} = \nu_{xz} = \frac{C_{12}}{C_{11} + C_{12}}, \quad (6c)$$

where the C_{ij} are elastic constants of crystalline silver. The values used are $C_{11} = 122.27$ GPa, $C_{12} = 91.77$ GPa, and $C_{44} = 46.06$ GPa and density $\rho = 10.5$ g/cm³.⁴⁶ The density is taken to be isotropic.

The above analysis makes no assumptions regarding the importance of different modes and, therefore, implicitly determines the relative contribution of all modes. In the following, the modes are labeled by whether they are singly (a), doubly (e), or triply degenerate (t), and numbered according to increasing energy. This nomenclature is appropriate for the O_h point group of the cubes.⁴⁷ We present Fourier coefficients for the relative contribution of all modes to the displacement, as given by α_n , and to the change in volume, as given by γ_n . Figure 6 shows the Fourier coefficients of deformation and of change in volume versus normalized frequency $\bar{\omega} = \omega L \sqrt{\rho/E}$ from the theoretical analysis for the initial uniform strain. These results show that the deformation and volume changes are dominated by two distinct modes: mode $\nu_{17}(a)$, which has a normalized eigenfrequency of $\bar{\omega} = 6.04$, and mode $\nu_{42}(a)$, which has a normalized eigenfrequency of $\bar{\omega} = 9.31$. The shapes of these two modes are pre-

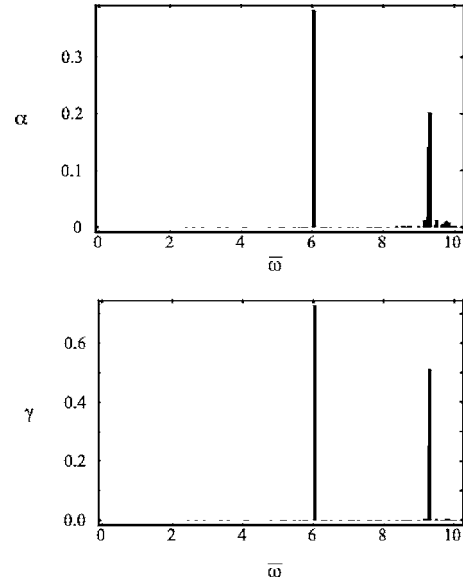


FIG. 6. Fourier coefficients for the displacement α_n and volume change γ_n associated with the n th mode vs normalized frequency $\bar{\omega} = \omega L \sqrt{\rho/E}$ for a uniform initial strain.

sented in Fig. 7. It is clear that these modes correspond to the fundamental and overtone breathing vibrations. The periods corresponding to these two modes are plotted in Fig. 5 as the solid lines for the actual dimensions of the cubes studied.

Since the optical penetration depth in metals is typically of the order of 10–20 nm,³⁷ nonuniform heating effects can occur in our experiments,^{48–50} especially for the larger particles. Nonuniform heating produces a nonuniform initial stress field, which induces a nonuniform initial strain field.^{48–50} Importantly, the time scale for thermal diffusion in the interior of the cube is small in comparison to the time scale of the fundamental resonant vibrations. As such, any nonuniform excitation in this system will rapidly relax into uniform excitation before any significant vibrational displacement occurs. This feature then allows the nonuniform heating to be modeled by an impulsive strain. In the frequency domain, this impulsive strain in time becomes a frequency independent strain. As such, the dominant modes excited by this nonuniform impulsive excitation can be obtained in an analogous manner to that for uniform excitation, by imposing a spatially varying strain field in the fre-

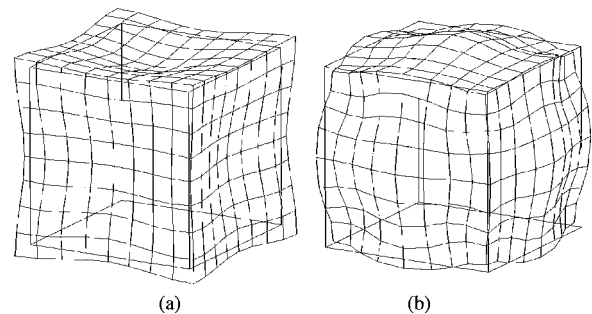


FIG. 7. Mode shapes for the two dominant modes observed in Fig. 6. (a) Mode shape of the 17th eigenmode, which has a normalized eigenfrequency of $\bar{\omega} = 6.04$. (b) Mode shape of the 42nd eigenmode, which has a normalized eigenfrequency of $\bar{\omega} = 9.31$.

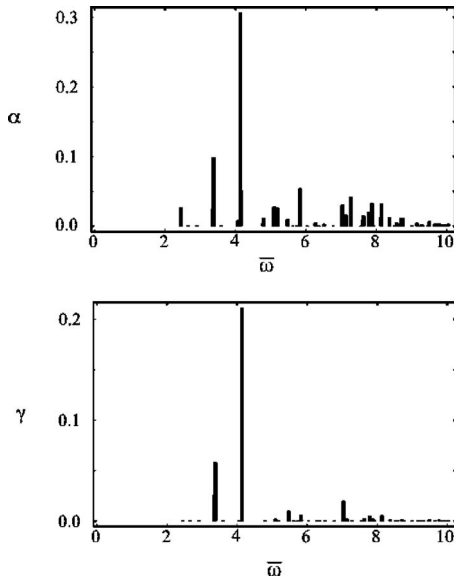


FIG. 8. Fourier coefficients for the displacement α_n and volume change γ_n associated with the n th mode vs normalized frequency $\bar{\omega} = \omega L \sqrt{\rho/E}$ for a nonuniform initial strain [as given by Eq. (7)].

quency domain. We model this effect here by considering that the initial strain decays exponentially with distance from one side of the cube.⁵¹ The specific displacement field used is

$$\mathbf{U}_{t=0} = \begin{cases} \mathbf{0}, & x \leq 0 \\ \varepsilon \frac{2^{2x} - 1}{2} (\hat{y} + \hat{z}), & x > 0. \end{cases} \quad (7)$$

The modes excited are then evaluated in an identical manner to that of uniform heating by use of Eqs. (3) and (5).

Note that Eq. (7) corresponds to a situation where the pump laser beam is normal to a surface of the particle. However, in solution the cubes are randomly orientated and so, in principle, many different nonuniform initial strain fields should be considered. However, the simple model given in Eq. (7) is expected to capture the basic physics of this situation and allow determination of the modes excited by nonuniform heating. Results of the analysis using the initial strain field described by Eq. (7) are given in Fig. 8.

Comparing Figs. 6 and 8, we observe that the modes excited by nonuniform heating differ considerably to those for uniform heating. This is not surprising, since the uniform initial strain only excites totally symmetric vibrational modes, whereas the nonuniform strain excites nontotally symmetric modes. The two dominant modes that appear in the deformation and volume change for nonuniform heating are both triply degenerate: mode $\nu_5(t)$ with a normalized eigenfrequency of $\bar{\omega} = 3.38$ and mode $\nu_8(t)$ which has an eigenfrequency of $\bar{\omega} = 4.14$. A triply degenerate mode has three mode shapes, which have the same shape but different direction. One component of the two dominant degenerate modes [$\nu_5(t)$ and $\nu_8(t)$] is shown in Fig. 9. Note that these modes possess frequencies that are significantly lower than those of the symmetric modes excited by uniform heating, and the mode shapes for uniform and nonuniform excitations

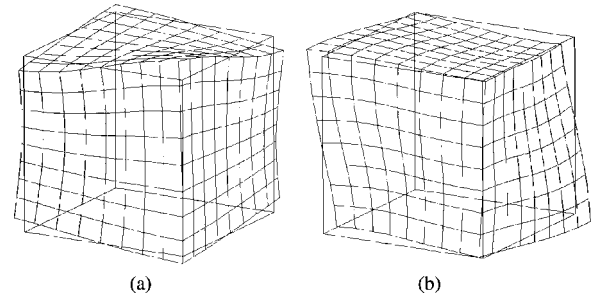


FIG. 9. Mode shapes for the two dominant modes observed in Fig. 8. (a) Mode shape of the fifth eigenmode, which has a normalized eigenfrequency of $\bar{\omega} = 3.38$. (b) Mode shape of the eighth mode, which has a normalized eigenfrequency of $\bar{\omega} = 4.14$. Both these modes are triply degenerate and only one component is shown.

also differ considerably. The periods for the main modes excited by nonuniform heating are shown in Fig. 5 as the dashed lines.

IV. DISCUSSION

Inspection of Fig. 5 shows that the higher frequency modulations observed for the cubes can be assigned to the breathing mode ($\nu_{17}(a)$), and the lower frequency modulations can be assigned to a mode that arises from nonuniform heating ($\nu_8(t)$). A more quantitative comparison of theory and experiment can be made by using the experimental data to calculate normalized eigenfrequencies. We find $\bar{\omega} = 5.60 \pm 0.15$ for the high frequency mode and $\bar{\omega} = 4.25 \pm 0.08$ for the low frequency mode. These values are essentially within experimental error of the calculated values of $\bar{\omega} = 6.04$ for $\nu_{17}(a)$ and $\bar{\omega} = 4.14$ for $\nu_8(t)$. This shows that the vibrational response of cubic particles to ultrafast laser-induced heating can be well described by continuum mechanics, and that the elastic constants of the particles are the same as bulk silver (to within the accuracy of our measurements). This is the main result of this paper, and is in agreement with the recent study of the vibrational response of single crystal Ag triangles by Bonacina *et al.*²⁶ However, the observation of bulk elastic properties for nanoparticles is in contrast to our experiments with gold nanorods, where we found that the value of Young's modulus for the rods was significantly smaller than the value for bulk gold.^{29,30,43} At this point it is not clear why the nanorods show different properties compared to bulk material.

The relative phase of the vibrational modulations observed in Figs. 3 and 4 is also an interesting issue in these experiments. The phase depends on whether the vibrations are excited by a displacive (step-function-like)⁵² or an impulsive (delta-function-like) mechanism.^{53,54} Whether the initial strains caused by laser-induced heating are displacive or impulsive depends on the time scale for their decay compared to the periods of the vibrational modes. The uniform initial strain decays via heat dissipation in the surroundings, which is a long time scale process.⁴⁵ Thus, this effect corresponds to a displacive excitation. The nonuniform initial strain decays via internal heat diffusion in the particle, the time scale of which is given by $\tau = L^2/D$, where $D = \kappa/C$ is the thermal diffusivity, κ is the thermal conductivity,

ity, and C is the heat capacity.^{48–50} The thermal diffusivity for silver is approximately $170 \text{ nm}^2/\text{ps}$,⁵⁵ thus, for our particles the internal heat diffusion time is faster than the period of the low frequency modes [$\nu_5(t)$ and $\nu_8(t)$] for all sizes ($L=30\text{--}100 \text{ nm}$). This implies that the nonuniform strain gives an impulsive excitation mechanism and, therefore, that the vibrational motions excited by the uniform and nonuniform strains should be 90° out of phase.^{26,53,54} This is indeed observed for sample S4 in Fig. 3, where the average phase difference over all the wavelengths where the two modulations are observed is 95° . However, the phase of the modulations detected in the transient absorption traces also depends on the details of how the excited mode affects the optical spectrum and the specific probe wavelength.^{40,56} Thus, the observation that the phases of the two vibrational modes are similar for sample S6 does not necessarily disprove that the nontotally symmetric mode ($\nu_8(t)$) is excited by an impulsive mechanism. For this sample we may simply be at a wavelength where the two phases are equal.²⁶ Unfortunately, we were not able to record high quality transient absorption traces over a wide range of wavelengths for this sample.

Multiple coherently excited vibrational modes with different phases, arising from impulsive versus displacive excitation, have recently been observed for silver triangles.²⁶ However, in these experiments the two modes had the same symmetry (totally symmetric). The lower frequency mode (which mainly involves motion in the plane of the triangle) was excited by laser-induced thermal expansion (displacive). The higher frequency mode (out-of-plane motion) was excited by hot-electron pressure.²⁶ Hot-electron pressure gives an impulsive excitation mechanism.^{53,54} This effect is more important for the out-of-plane motion because the thickness of the triangles is much less than their edge length, and is less than the mean free path of the electrons.⁵⁴ This result is somewhat different than our case, where the excited modes have different symmetries, and the proposed excitation mechanisms involve a uniform initial strain versus a nonuniform initial strain. A nonuniform initial strain may also be responsible for the excitation of nontotally symmetric vibrational modes observed in the single particle experiments on spherical gold particles by van Dijk *et al.*⁵⁷

The last point considered here is the decay time of the two vibrational modes. For both samples S4 and S6 the lifetime of the higher frequency mode is much shorter than that of the lower frequency mode. If the decay times were solely determined by polydispersity, then one would expect the ratio of the decay time (τ) to the period (T) to be constant: specifically, it can be shown that $\tau/T = \langle L \rangle / \sqrt{2} \pi \sigma_L$ where σ_L is the standard deviation for the dimension L .⁵⁸ This expression does not correctly describe the present experiments. The high frequency mode decays much faster than expected (see Figs. 3 and 4). This suggests that the higher frequency motions for the cubes may be subjected to additional decay mechanisms, such as internal vibrational energy redistribution (energy flow out of high frequency modes into low frequency modes). Experiments are currently underway to investigate the vibrational lifetimes in these systems.

V. SUMMARY AND CONCLUSIONS

Time-resolved spectroscopy has been used to investigate the response of silver nanocubes to ultrafast laser-induced heating. Modulations due to two vibrational modes appear in the experimental traces. Comparing the experimental results to finite element calculations allows us to assign the higher frequency mode to the breathing mode of the particles ($\nu_{17}(a)$) and the lower frequency mode to a nontotally symmetric mode [which we label as $\nu_8(t)$]. The breathing mode is excited by the uniform initial strain created by lattice heating, which persists for much longer than the time scale of the vibrational motion (its decay is controlled by heat dissipation in the environment). This corresponds to the usual displacive excitation mechanism seen in these types of experiments.^{22,23} On the other hand, we believe that the nontotally symmetric mode is excited by a nonuniform initial strain that is generated from uneven pump laser absorption (this mode is only observed for particles much larger than the optical skin depth of the pump laser). A nonuniform initial strain will decay on a very fast time scale due to internal heat diffusion and, therefore, should give rise to an impulsive excitation mechanism. However, the sample polydispersity and the complicated nature of the vibrational motions do not allow this effect to be quantitatively analyzed in these experiments. Overall, the good agreement between the calculated and experimental vibrational frequencies shows that the elastic constants of these particles are the same as bulk silver.

ACKNOWLEDGMENTS

This work has been supported in part by a DARPA-DURINT subcontract from Harvard University and the David and Lucile Packard Foundation. One of the authors (Y.X.) is an Alfred P. Sloan Research Fellow and a Camille Dreyfus Teacher Scholar. Another authors (G.V.H.) acknowledges the support of the NSF (Grant No. CHE02-36279), and the Petroleum Research Fund (Grant No. PRF-39761AC) administered by the American Chemical Society. The work in Australia was supported by the Particulate Fluids Processing Centre and the Australian Research Council grants scheme. The authors would also like to thank Prashant Kamat and Istvan Robel for their help in collecting the time and wavelength resolved data in Fig. 3.

- ¹P. Pawlow, *Z. Phys. Chem.* **65**, 1 (1909); **65**, 545 (1909).
- ²P. Buffat and J. P. Borel, *Phys. Rev. A* **13**, 2287 (1976).
- ³R. Kofman, P. Cheyssac, A. Aouaj, Y. Lereah, G. Deutscher, T. Ben-David, J. M. Penisson, and A. Bourret, *Surf. Sci.* **303**, 231 (1994).
- ⁴K. Dick, T. Dhanasekaran, Z.-Y. Zhang, and D. Meisel, *J. Am. Chem. Soc.* **124**, 2312 (2002).
- ⁵S. H. Tolbert and A. P. Alivisatos, *Science* **265**, 373 (1994).
- ⁶S. H. Tolbert, A. B. Herhold, L. E. Brus, and A. P. Alivisatos, *Phys. Rev. Lett.* **76**, 4384 (1996).
- ⁷L. E. Brus, *J. Chem. Phys.* **80**, 4403 (1984).
- ⁸C. B. Murray, D. J. Norris, and M. G. Bawendi, *J. Am. Chem. Soc.* **115**, 8706 (1993).
- ⁹M. Haruta, *Catal. Today* **36**, 153 (1997).
- ¹⁰M. Valden, X. Lai, and D. W. Goodman, *Science* **281**, 1647 (1998).
- ¹¹M. C. Daniel and D. Astruc, *Chem. Rev. (Washington, D.C.)* **104**, 293 (2004).
- ¹²X. G. Peng, L. Manna, W. D. Yang, J. Wickham, E. Scher, A. Kadavanch, and A. P. Alivisatos, *Nature (London)* **404**, 59 (2000).
- ¹³N. R. Jana, L. Gearheart, and C. J. Murphy, *J. Phys. Chem. B* **105**, 4065

- (2001).
- ¹⁴ B. Nikoobakht and M. A. El-Sayed, *Chem. Mater.* **15**, 1957 (2003).
- ¹⁵ R. C. Jin, Y. W. Cao, C. A. Mirkin, K. L. Kelly, G. C. Schatz, and J. G. Zheng, *Science* **294**, 1901 (2001); R. C. Jin, Y. W. Cao, E. C. Hao, G. S. Metraux, G. C. Schatz, and C. A. Mirkin, *Nature (London)* **425**, 487 (2003).
- ¹⁶ A. Callegari, D. Tonti, and M. Chergui, *Nano Lett.* **3**, 1565 (2003).
- ¹⁷ Y. G. Sun and Y. N. Xia, *Science* **298**, 2176 (2002).
- ¹⁸ L. Manna, E. C. Scher, and A. P. Alivisatos, *J. Am. Chem. Soc.* **122**, 12700 (2000).
- ¹⁹ M. B. Mohamed, D. Tonti, A. Al Salman, and M. Chergui, *ChemPhysChem* **6**, 2505 (2005).
- ²⁰ E. Hao, R. C. Bailey, G. C. Schatz, J. T. Hupp, and S. Y. Li, *Nano Lett.* **4**, 327 (2004).
- ²¹ C. L. Nehl, H. W. Liao, and J. H. Hafner, *Nano Lett.* **6**, 683 (2006).
- ²² C. Voisin, N. Del Fatti, D. Christofilos, and F. Vallee, *J. Phys. Chem. B* **105**, 2264 (2001).
- ²³ J. H. Hodak, A. Henglein, and G. V. Hartland, *J. Phys. Chem. B* **104**, 9954 (2000).
- ²⁴ G. Cerullo, S. De Silvestri, and U. Banin, *Phys. Rev. B* **60**, 1928 (1999).
- ²⁵ W. Y. Huang, W. Qian, and M. A. El-Sayed, *J. Phys. Chem. B* **109**, 18881 (2005).
- ²⁶ L. Bonacina, A. Callegari, C. Bonati, F. van Mourik, and M. Chergui, *Nano Lett.* **6**, 7 (2006).
- ²⁷ D. H. Son, J. S. Wittenberg, U. Banin, and A. P. Alivisatos, *J. Phys. Chem. B* **110**, 19884 (2006).
- ²⁸ L. D. Landau and E. M. Lifshitz, *Theory of Elasticity*, 2nd ed. (Pergamon, Oxford, NY, 1970).
- ²⁹ M. Hu, P. Hillyard, G. V. Hartland, T. Kosel, J. Perez-Juste, and P. Mulvaney, *Nano Lett.* **4**, 2493 (2004).
- ³⁰ H. Petrova, J. Perez-Juste, Z. Zhang, J. Zhang, T. Kosel, and G. V. Hartland, *J. Mater. Chem.* **16**, 3957 (2006).
- ³¹ Z. L. Wang, M. B. Mohamed, S. Link, and M. A. El-Sayed, *Surf. Sci.* **440**, L809 (1999).
- ³² F. Kim, J. H. Song, and P. D. Yang, *J. Am. Chem. Soc.* **124**, 14316 (2002).
- ³³ C. K. Tsung, X. Kou, Q. Shi, J. Zhang, M. H. Yeung, J. Wang, and G. D. Stucky, *J. Am. Chem. Soc.* **128**, 5352 (2006).
- ³⁴ C. J. Johnson, E. Dujardin, S. A. Davis, C. J. Murphy, and S. Mann, *J. Mater. Chem.* **12**, 1765 (2002).
- ³⁵ H. Hofmeister, S. A. Nepijko, D. N. Ievlev, W. Schulze, and G. Ertl, *J. Cryst. Growth* **234**, 773 (2002).
- ³⁶ M. Liu and P. Guyot-Sionnest, *J. Phys. Chem. B* **109**, 22192 (2005).
- ³⁷ N. W. Ashcroft and N. D. Mermin, *Solid State Physics* (Rinehart, New York, 1976).
- ³⁸ S. H. Im, Y. T. Lee, B. Wiley, and Y. N. Xia, *Angew. Chem., Int. Ed.* **44**, 2154 (2005).
- ³⁹ U. Kreibig and M. Volmer, *Optical Properties of Metal Clusters* (Springer-Verlag, Berlin, 1995).
- ⁴⁰ G. V. Hartland, *Phys. Chem. Chem. Phys.* **6**, 5263 (2004).
- ⁴¹ G. V. Hartland, M. Hu, O. Wilson, P. Mulvaney, and J. E. Sader, *J. Phys. Chem. B* **106**, 743 (2002).
- ⁴² L. J. Sherry, S. H. Chang, G. C. Schatz, R. P. Van Duyne, B. J. Wiley, and Y. N. Xia, *Nano Lett.* **5**, 2034 (2005).
- ⁴³ M. Hu, X. Wang, G. V. Hartland, P. Mulvaney, J. Perez-Juste, and J. E. Sader, *J. Am. Chem. Soc.* **125**, 14925 (2003).
- ⁴⁴ LUSAS is a trademark and trading name of Finite Element Analysis Ltd., Forge House, 66 High Street, Kingston upon Thames, Surrey, KT1 1HN, UK.
- ⁴⁵ M. Hu and G. V. Hartland, *J. Phys. Chem. B* **106**, 7029 (2002).
- ⁴⁶ G. Simmons and H. Wang, *Single Crystal Elastic Constants and Calculated Aggregate Properties: A Handbook* (MIT, Cambridge, 1971).
- ⁴⁷ D. M. Bishop, *Group Theory and Chemistry* (Dover, New York, 1993).
- ⁴⁸ C. Thomsen, H. T. Grahn, H. J. Maris, and J. Tauc, *Phys. Rev. B* **34**, 4129 (1986).
- ⁴⁹ O. B. Wright, *Phys. Rev. B* **49**, 9985 (1994).
- ⁵⁰ G. Tas and H. J. Maris, *Phys. Rev. B* **49**, 15046 (1994).
- ⁵¹ A complete and rigorous analysis would require a solution of the coupled optical-thermal-elastic problem, which is beyond the scope of the present work.
- ⁵² H. J. Zeiger, J. Vidal, T. K. Cheng, E. P. Ippen, G. Dresselhaus, and M. S. Dresselhaus, *Phys. Rev. B* **45**, 768 (1992).
- ⁵³ M. Perner, S. Gresillon, J. Marz, G. von Plessen, J. Feldmann, J. Porstendorfer, K. J. Berg, and G. Berg, *Phys. Rev. Lett.* **85**, 792 (2000).
- ⁵⁴ C. Voisin, N. Del Fatti, D. Christofilos, and F. Vallee, *Appl. Surf. Sci.* **164**, 131 (2000).
- ⁵⁵ *American Institute of Physics Handbook*, 3rd ed. (McGraw-Hill, New York, 1972).
- ⁵⁶ G. V. Hartland, *Annu. Rev. Phys. Chem.* **57**, 403 (2006).
- ⁵⁷ M. A. van Dijk, M. Lippitz, and M. Orrit, *Phys. Rev. Lett.* **95**, 267406 (2005).
- ⁵⁸ G. V. Hartland, *J. Chem. Phys.* **116**, 8048 (2002).